Biomass Conversion and Biorefinery (2024) 14:19489–19500
https://doi.org/10.1007/s13399-023-03959-7

ORIGINAL ARTICLE

Preparation and characterization of cellulose/ZnO nanoparticles extracted from peanut shells: effects on antibacterial and antifungal activities

Hafidha Terea[1] · Djamel Selloum[2] · Abdelkrim Rebiai[3] · Abderrhmane Bouafia[4] · Omar Ben Mya[4]

Received: 2 January 2023 / Revised: 10 February 2023 / Accepted: 14 February 2023 / Published online: 22 February 2023

Abstract

This work aims to recycle peanut shells (residues) to use them as raw materials to produce nanocrystal cellulose. Two methods were used to synthesis zinc oxide nanoparticles (ZnO NPs) on cellulose nanocrystals (CNCs), in order to form the cellulose/zinc oxide nanoparticles (CNC/ZnO NPs). According to the results, Fourier transform infrared, X-ray diffraction, UV–visible, scanning electron microscopy, and energy-dispersive X-ray analysis characterized the CNC/ZnO NPs. UV-Visble spectra showed maximum absorption at 366 nm related to the zinc oxide. Fourier transform infrared spectra exhibit a weak peak at 432 cm^{-1} attributed to zinc oxide vibration, confirming the formation of zinc oxide nanoparticles on cellulose nanocrystals. X-ray diffraction confirmed the crystalline nature of cellulose/zinc oxide nanoparticles with an average size between 20 and 28 nm. Scanning electron microscopy survey shows that the obtained nanoparticles have a lattice shape of rods surrounded by zinc oxide nanoparticles with a hexagonal wurtzite structure, as established by energy-dispersive X-ray analysis to confirm the presence of carbon, zinc, and oxygen. These cellulose/zinc oxide nanoparticles were tested against human pathogenic bacteria (*Escherichia coli* ATCC25922, *Klebsiella pneumoniae* ATCC 10,031, *Staphylococcus aureus* ATCC 25,923) and a fungus (*Candida albicans* ATCC 14,053). The obtained results revealed that these cellulose/zinc oxide nanoparticles synthesized from peanut shells have the effectiveness of an antibacterial activity against Gram (+) and Gram (−) bacteria together, and it shows excellent antifungal activity against *Candida albicans*; it seems to have an immense potential as the source of antibacterial and antifungal compounds. These results indicate that these newly fabricated cellulose/zinc oxide nanoparticle bio-nanocomposites by both methods contain potential antimicrobial components that may be of great benefit in the development of antimicrobial pharmaceutical industries and can be used as a treatment against various diseases caused by these organisms. It can also be employed in food systems as a novel preservative to inhibit microbial growth and repress the synthesis of exotoxins or control the growth of spoilage and disease-causing microorganisms.

Keywords Peanut shells · Cellulose nanocrystals · ZnO · Characterized · Antibacterial activity · Antifungal activity

Abbreviations

Cs	*celluloses*
CNCs	*cellulose nanocrystal*
ZnO	*zinc oxide*
CNC/ZnO NPs	*cellulose/zinc oxide nanoparticule*
M1and M2	*method 1 and method 2*
CrI	*crystallinity index*
CrS	*crystalline size*

✉ Hafidha Terea
terea.hadile88@gmail.com

✉ Abderrhmane Bouafia
abdelrahmanebouafia@gmail.com

Djamel Selloum
selloumdjamel@gmail.com

Abdelkrim Rebiai
new.rebiai@gmail.com

Omar Ben Mya
obenmya@yahoo.fr

[1] Department of Process Engineering, LVPRS, University of Kasdi Merbah, 30000 Ouargla, Algeria

[2] Laboratoire Croissance et Caractérisation de Nouveaux Semi-conducteurs, Université Ferhat Abbas, 19000 Sétif-1, Algérie

[3] Department of Chemistry, Faculty of Exact Sciences, University of Echahid Hamma Lakhdar El-Oued, 39000 El-Oued, Algeria

[4] Department of Process Engineering and Petrochemistry, Faculty of Technology, University of El-Oued, 39000 El-Oued, Algeria

ZNI *zones inhibitions*
DMSO *dimethyl sulfoxide*

1 Introduction

The appearance and development of nanotechnology have brought new possibilities and broader perspectives to the world, as well as allowing people to achieve further goals by manipulating materials at the nanometer scale; it has triggered a paradigm shift in global life due to its application in several fields [1, 2]. Through the many numbers of existing nanoparticles, metal oxide nanoparticles are considered to be the most used due to their physical, chemical, and biological properties [3–5].

Zinc oxide (ZnO) is a semiconductor material. It has a direct wide bandgap of 3.37 eV and a large binding energy of 60 meV at room temperature. ZnO NPs are commonly used in modern nanotechnology research because of their physical and chemical properties, and wide range of applications, such as oleic acid batteries [6], gas sensors and catalysts [7–10], and antibacterial agents [11]. Also, it is an effective bactericide against Gram-positive and Gram-negative bacteria [12, 13]. ZnO NPs have been reported to disrupt membrane structure and alter permeability, thereby accumulating in the cytoplasm of bacteria [14].

The agricultural domain annually produces large quantities of plant waste which pollutes the environment and contains a high percentage of cellulose. Cellulose is one of the most abundant natural polymers [15], because it is derived from renewable, biodegradable, non-toxic, and inexpensive sources [16, 17]. CNCs are characteristically rod-formed monocrystals, 1 to 100 nm in diameter [18].

CNCs can be produced from various agricultural wastes by many extraction methods like high-pressure mechanical [19], enzymatic hydrolysis [20], acid hydrolysis [21], and ultrasound of ultrasonication [22].

CNCs show such outstanding properties as a large aspect ratio [23], minimal thermal degradation behavior [24], good mechanical properties [25], and a big capacity for absorption of metallic particles [26]. Can be used in bio-energy, chemical, catalytic, and biomedical applications [27].

Peanut (*Arachis hypogaea* L.) [28] is a leguminous plant of the Arachis genus, native to Central and South America, and is an important and abundant agricultural product in many countries [29, 30], especially Algeria, for human and animal production; mass consumption is widespread in many different forms of food.

The aim of this study was to evaluate the CNCs produced from peanut shells in the wilaya of El-Oued (Algeria). The CNC extraction method used in this study is a combination of acid hydrolysis and ultrasound of ultrasonication. Also in this work, we synthesized CNC/ZnO NPs in two different methods by loading ZnO NPs on the CNCs to obtain the correct component (CNC/ZnO NPs). The resulting CNC/ZnO NPs were characterized using Fourier transform infrared spectroscopy, scanning electron microscopy (SEM), X-ray diffraction, and ultraviolet–visible spectroscopy (UV). In addition, this study also evaluates the antibacterial and antifungal activities of the resulting nanoparticles.

2 Experimental section

2.1 Materials

Peanut shells were collected from the city of El-Oued in Algeria. Hydrochloric acid (HCl, BioChem, 37%), sodium hydroxide (NaOH, BioChem, 99%), sodium hypochlorite ($NaClO_2$, 99%), sulfuric acid (H_2SO_4, BioChem, 96%), urea (CH_4N_2O, Sigma-Aldrich, 99%), zinc nitrate ($Zn(NO_3)_2$, BioChem, 99.7%), dimethyl sulfoxide ($(CH_3)_2SO$, Sigma-Aldrich, 99.9%), and zinc chloride ($ZnCl_2$, Sigma-Aldrich, 98%) were used as received.

Bacteria *Escherichia coli* (ATCC25922), *Klebsiella pneumoniae*(ATCC 10,031), and *Staphylococcus aureus* (ATCC 25,923) and one species of yeast *Candida albicans* (ATCC 14,053).

2.2 Preparation of cellulose/zinc oxide nanoparticules

2.2.1 Isolation of cellulose

Peanut shells were repeatedly washed using water to remove impurities and dried at a controlled temperature (60 °C for 72 h). After drying, they were grounded in an electric mill and classified by a 500-µm sieve.

The shells are first rinsed with hot water, using a (W/V) (1:6)/(g: ml) adapter at 100 °C for 15 min to remove some compounds such as waxes, phenolic compounds, sugars, and water-soluble polysaccharides. Then, the treated shells were dried at 50 °C for 12 h. Then, the waste was treated with HCl solution (1 M) at 85 °C for 30 min to remove acid-soluble substances. After that, the residue was filtered and washed several times with deionized water until the pH was neutral, followed by a basic treatment with NaOH solution (1 M) at 85 °C for 1 h to partially remove hemicellulose and lignin. Lastly, the residue was filtered and rinsed several times with deionized water to neutral pH, followed by 3 times of bleaching with $NaClO_2$ solution (2%) at 95 °C for 1 h. Finally, the cellulose fibers were obtained by centrifuge separation. The precipitate was washed several times with deionized water and passed through a centrifuge (5000 rpm; 15 min) to neutral pH. Fibers were sonicated for 20 min and dried in a convection oven at 65 °C for 24 h [31].

2.2.2 Preparation of cellulose nanocrystals

Cellulose nanocrystal (CNCs) was isolated by hydrolyzing cellulose fibers (1 g) with 50 ml sulfuric acid solution (H_2SO_4) with different concentrations (C_{H2SO4} = 40%, 38%, and 36%), respectively, at room temperature for 4 h [32]. The resultant suspension was diluted 10 times with cold water (4 °C). Followed by centrifuge at 5000 rpm to reduce its water content and washed until a neutral pH. Finally, the samples of CNCs obtained were treated with ultrasound of ultrasonication and dried at 50 °C.

2.3 Syntheses of CNC/ZnO NPs

In this work, two methods to synthesis the CNC/ZnO NPs were used.

2.3.1 The first method (CNC/ZnO NPs.M1)

Modified protocols from previous studies were used for the synthesis of CNC/ZnO NPs by a green method using plant extract [33–39]. In this method, we prepared a mixed aqueous solution to dissolve CNCs by directly mixing distilled water, NaOH, and urea. The concentrations of NaOH and urea were respectively, 7% and 12%. All concentrations were calculated by weight percent [40]. The quantity of dried CNCs was immersed in the solvent and stirred at ambient temperature for about 30 min until it became transparent without any natural fibers cellulose solution; cellulose is considered to be completely dissolved. The mixture was then cooled to − 20 °C for 17 h. After 17 h, the mixture was heated and melted to 80 °C, and zinc nitrate solution (50 mM) was added dropwise (by the gel solution method) to the dissolved mixture solution until the color changed to milky white. The reaction was carried out at 80 °C for 4 h using reflux with continuous gentle stirring. We then stopped the reaction by diluting and cooling the mixture.

2.3.2 The second method (CNC/ZnO NPs.M2)

For this method, we used CNCs as the insoluble solid. In the reflux assembly, 1 g of CNCs milled to $ZnCl_2$ solution was added (50 mL/0.2 M), stirring and heating the mixture to 80 °C (about 30 min).

After 30 min, NaOH solution (50 ml/1 M) was added dropwise to the mixture, then continue the stirring and heating at the same temperature, 80 °C, for 2 h. After that, the mixture was cooled and the precipitate was recovered using a centrifuge.

The white solid products (CNC/ZnO NPs) of the two methods were collected separately by centrifugation (5000 t/min, 10 min) at room temperature and washed several times with distilled water to make the pH neutral. It was then sonicated for 30 min and dried at 70 °C to completely convert the remaining zinc hydroxide to zinc oxide.

2.4 Characterization of CNC/ZnO NPs

The characterization of CNC/ZnO NPs depended on the use of the following techniques: FT-IR, XRD, UV–Vis, SEM, and energy-dispersive X-ray analysis (EDAX).

2.4.1 Fourier transform infrared spectroscopy

Raw materials, purified cellulose, and CNC/ZnO NPs were analyzed using Fourier transform infrared spectroscopy. Analysis was performed using an Agilent Cary 630 FTIR instrument to examine functional group changes due to cellulose purification, preparation of CNCs/ZnO NPs, and comparison between samples. Spectra were collected under the following conditions, with a quantity range of 4000–400 cm^{-1}, 16 scan samples, 16 background scans, and a resolution of 16 cm^{-1}.

2.4.2 X-ray diffraction analysis

X-ray diffraction spectra were obtained using X-ray diffraction to observe the diffraction patterns of all developed samples (XRD, Mini Flex 600 Rigaku) with Cu-kα radiation at Cu-k and wavelength (λ = 1.5418 Å). Data were collected at 2θ values between 10° and 80° and room temperature.

The crystallinity index (CrI) of cellulose was calculated from the XRD patterns according to the Segal method [41]:

$$\mathrm{CrI}(\%) = \left(\left(\mathrm{I}_{002} - \mathrm{I}_{am}\right)/\mathrm{I}_{002}\right) \times 100 \quad (1)$$

where I_{002} is the maximum (002) lattice diffraction intensity at 2θ = 23.0° and I_{am} is the diffraction intensity at 2θ = 18°.

Calculate crystal size using Scherer's equation [42, 43].

$$CrS = (k \times \lambda)/(\beta \times cos\theta) \quad (2)$$

where K = constant = 0.91, λ is the X-ray wavelength = 1.5418, θ = Bragg angle, and β = full width at half maximum intensity of the high-intensity peak corresponding to the diffraction level.

2.4.3 UV–visible absorption spectroscopy

UV–Vis absorption spectroscopy plays a very important role in examining the optical properties of nanoparticles [44]. The optical properties of CNC/ZnO NPs were studied using UV–visible transmittance spectroscopy by means of Shimadzu device (the device was Shimadzu-1800, Japanese UV–vis spectrophotometer) worked in the wavelength range of 200–900 nm. The analysis was performed in a quartz cell using distilled water as the reference solvent.

2.4.4 Scanning electron microscope

The morphology of the CNC/ZnO NPs was investigated using a scanning electron microscope (SEM-TESCAN VEGA 3) equipped with EDAX at an accelerating voltage of 20 kV.

2.5 Evaluate the antimicrobial and antifungal activities of CNCs/ZnO NPs

Agar well diffusion method has been used to determine the antimicrobial activities of different samples extracted from peanut shells (CNC, CNC/ZnO NPs.M1, and CNC/ZnO NPs.M2) each sample at a concentration of 20 mg/ml in DMSO solution [45], against Gram-positive bacteria (*Staphylococcus aureus*), Gram-negative bacteria (*Escherichia coli* and *Klebsiella pneumonia*), and one fungus (*Candida albicans*), which is similar to disk streaming. This method has been modified from [46].

Mueller Hinton agar applied for bacterial culture and Sapporo agar applied for yeast culture into a 90-cm Petri dish. From 18 to 24 h, small colonies were formed, making bacterial suspensions of each strain in 9 ml of sterile physiological water (diluted tenfold). After the agar has solidified in the petri dish, raked pipette was used to inoculate the surface with the bacterial suspension and spread the bacterial suspension with 100 µl of the dilution solution. Agar wells with a diameter of 6 mm were made in each of the agar plates using a sterile stainless steel cork borer and filled 50 µl of the sample. A standard antibiotic disk of *levofloxacin* (a reference antibiotic and antifungal drug) was used as a positive control, and a disk soaked in DMSO was used as a negative control. The test was performed twice, using an average of two sample wells during each test.

After overnight incubation at 37 °C. The diameter of the zone of inhibition (IZ) around the disk containing the sample to be tested was measured.

3 Results and discussion

3.1 FTIR spectroscopy

The FTIR analysis spectra of untreated and treated peanut hull fibers are shown in Fig. 1a, showing similar patterns in the range of 4000 to 400 cm^{-1}. The first absorption range of all samples is centered at 3650 to 3000 cm^{-1}, indicating hydrogen-bonded O–H groups [47, 48]. The presence of this hydroxyl group explains the presence of cellulose, lignin, and water in the fibers. Within this range, a reduction occurs in the hydrogen bonding strength of the cellulose hydroxyl groups, and thus, the hydrophilic behavior was also observed in all treated fibers. In the range between 2980

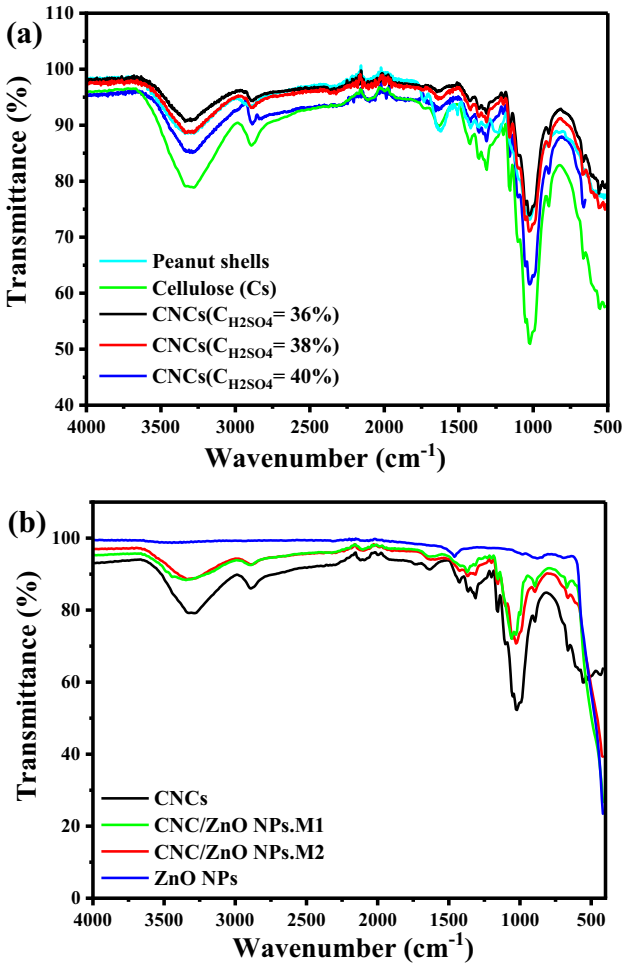

Fig. 1 FT-IR spectra (**a**) for CNCs isolated from peanut shells (C_{H2SO4} = 36%, 38%, and 40%); **b** for the composites CNC/ZnO NP synthesis from two methods (CNC/ZnO NPs.M1 and CNC/ZnO NPs.M2)

and 2800 cm^{-1} in the CNC spectrum, Trans, an indication that the number of –CH and –CH2 vibrations originating from the –CH and –CH2 nanobattery samples is increased [49]. The characteristic band of C–C has a benzene ring at 1634 cm^{-1} and a peak at 2886 cm^{-1}, corresponding to C–H stretching vibrations in cellulose, hemicellulose, and water [49–51].

The peak at 1734 cm^{-1} represents the C = O stretching in the lignin carboxylate bond, which may be related to the stretching vibration of the C = O group and the ester group in hemicellulose [50]. The peak at 1243 cm^{-1} for untreated fibers can be explained by the carbon dioxide stretching of acetyl groups in lignin [52, 53]. The peak observed at 1618 cm^{-1} is the result of water uptake [50, 54, 55].

We also noticed an improvement in peaks from the original sample (peanut shells) to other samples due to the removal of fat and non-cellulosic material after various chemical treatments. The 1156–896 cm^{-1} peaks show the

C–O–C bond vibration and C–H bond vibration of glucose, respectively [56, 57]. The peak at 1025 cm^{-1} in all spectra is due to the (1–4) D-glycosidic bond between the monosaccharide bands as an extension [50, 54, 58]. Due to the strong interaction between the oxygen atoms of CNCs and ZnO molecules, their absorption intensity increases throughout the treatment stages and shows a transition to higher wavenumbers and becomes broader [18, 59].

The absorption bands at 425 cm^{-1} and 432 cm^{-1} are shown in Fig. 1b which correspond to the stretching vibrations of Zn–O bonds in ZnO from CNC/ZnO NPs (M1 et M2) and match the spectra of pure ZnO. Small differences can also be observed between Zn–O adsorption bands due to variations in lattice parameters of ZnO NPs [60], and differences in Zn percentage in nanocomposite synthesis (confirmed by EDAX).

3.2 Crystal structure and composition

Figure 2a shows the XRD pattern of CNCs extracted from peanut shells. Three distinct main peaks were observed. An initial peak was detected at 2θ = 16°, at the lattice level (110), indicating the presence of amorphous components of cellulose and CNCs [51, 61–63].

It can be seen that the main sharp crystalline peaks for CNCs on each pattern are formed at about 2θ = 22° of the (002) lattice plane [51, 63–65]. The highest density of CNCs was in the samples treated with 40% of H_2SO_4 solution concentration. The peak appears at 2θ = 34° of the (004) lattice plane, which is due to the amorphous part of cellulose and CNCs [51, 63, 66].

Also, from XRD diffractograms, we determined the crystallinity index and crystal average size of extracted CNCs. According to Table 1, the higher CrI of the CNCs after acid treatment with concentration C_{H2SO4} = 40% is 77.95%, and the CrS is 8.88 nm. The reason for this is due to the reduction of cellulose chains after the removal of amorphous components such as hemicellulose, pectin, lignin, and impurities in the fibers, and the reduction of hydrophobicity after treatment [67, 68]. Therefore, this sample was approved for the assembly of CNC/ZnO NPs.

Figure 2b shows the XRD pattern of CNC/ZnO NPs.M1 and CNC/ZnO NPs.M2 synthesized from CNCs with ZnO NPs of peanut shells, which were synthesized by two different methods. The diffraction peaks are 2θ: 31.8°, 34.47°, 36.29°, 47.59°, 56.64°, 62.92°, 66.45°, 68.02°, and 69.16° corresponding to (100), (002), (101), (102), (110), (103), (200), (112), and (201) crystal planes [69]. All diffraction positions and relative intensity peaks are correctly set using JCPDS file card 0,361,451 and are in a good fit to the hexagonal ZnO wurtzite structure in previously reported work [69].

The CrS of CNC/ZnO NPs varied between 20.14 nm in the first method to 27.31 nm in the second method. The different properties of each method used lead to a different degree of stabilization of $Zn(OH)_2$ NPs against agglomeration of CNCs. This leads to the formation of ZnO NPs on the CNCs with the observed variation in its density (confirmed by DREX), crystallite size, and final shape of CNCs/ZnO NPs formed.

To obtain CNCs, here mild acid–alkali conditions were used for the fractioning process of biomass (peanut shells). Alkaline treatment in cellulose extraction leads to formation of crystals, which in turn leads to the disorder of fibrous crystals, which are considered amorphous because they

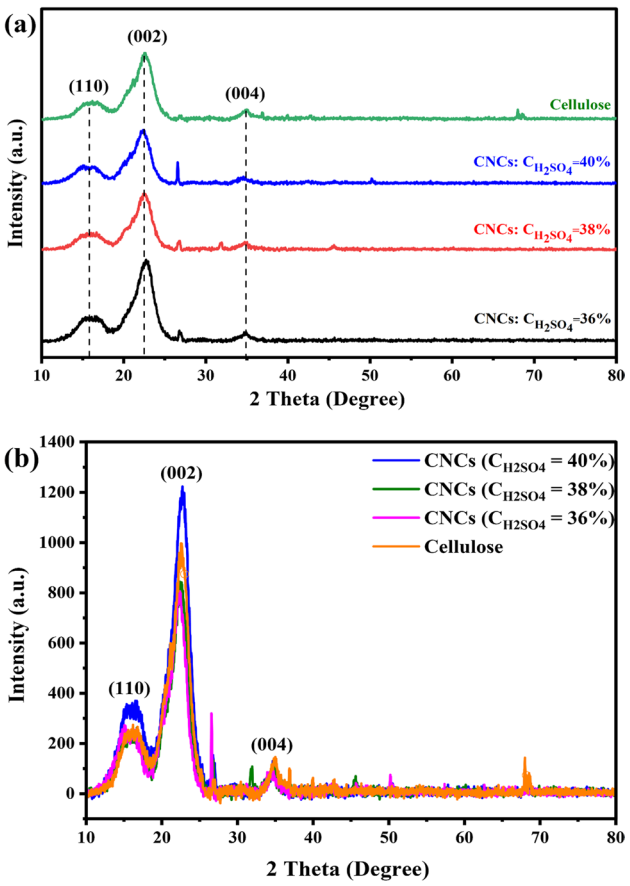

Fig. 2 XRD patterns of **a** CNCs (C_{H2SO4} = 36, 38, and 40%); **b** superimpose curves of CNCs (C_{H2SO4} = 36, 38, and 40%)

Table 1 Crystallization Index (CrI) and crystal size (CrS) of CNC/ZnO NPs

Samples	CNCs (36%)	CNCs (38%)	CNCs (40%)	CNC/ZnO NPs.M1	CNC/ZnO NPs.M2
CrI (%)	69.714	68.757	77.957	/	/
CrS (nm)	11.82	11.90	8.88	20.14	27.31

are not part of the crystals. Swelling of the structure due to penetration of the cellulose fibers by NaOH results in an increase in crystal size [70], while the acid treatment of HCl during the extraction of cellulose reduces the size of the crystals. This approach ensures the minimum degradation of valuable substances contained in biomass such as pectic and hemicellulosic polysaccharides.

Also, low-temperature process was chosen contrary to high-temperature hydrothermal processes in preparation of CNCs by the second acid treatment with H_2SO_4 solution. The polysaccharides are weakly bonded among each other and are packed in less structured tissue compared with peanut shell biomass. Hence, the low temperature is sufficient enough to improvement and miniaturization of cellulose crystal size which makes beneficial changes as it increases the specific surface area and water absorption capacity of bio-fibers, depending on their crystal size, as increasing crystal size can enhance the resistance to moisture absorption and chemical reactions of the fibers.

These characteristic peaks of pure ZnO observed in the XRD patterns confirm the formation and growth of ZnO NPs on CNC. Furthermore, XRD analysis also revealed that all recorded peak intensity distributions confirm the hexagonal writing structure of ZnO [70, 71]. Although the positions of the different ZnO peaks were similar for the two different methods, the width of the peaks decreased and the intensity of the peaks gradually increased by increasing ZnO content, indicating an increase in crystal size and crystallinity [72].

It can be seen that the reflection peaks are broadened in the samples synthesized by the first method, indicating that the particle size in the CNC/ZnO NPs.M1 is reduced and has more ZnO NPs (Fig. 3).

All the corresponding CNCs peaks can also be observed in samples with low intensities, especially in the first sample, which may be due to formation of a thick layer from ZnO NPs as a coating for CNCs (confirmed by SEM images), which results in a difficulty determining the value of the CrI.

3.3 Bandgap and optical properties

Figure. 4a shows the UV–Vis absorption spectra of CNC/ZnO NPs. UV–Vis spectroscopy revealed a maximum absorption near 366 nm, which may be an indicator of ZnO NP formation. This peak confirms the synthesis of pure ZnO NPs in the CNCs and the use of peanut shells to obtain CNC/ZnO NPs. Furthermore, it has been reported that the peak position of the UV–Vis spectrum correlates with nanoparticle size and color changes with decreasing nanoparticle crystal size [72].

The bandgap energy is calculated based on the numerical derivative of the optical absorption coefficient using the

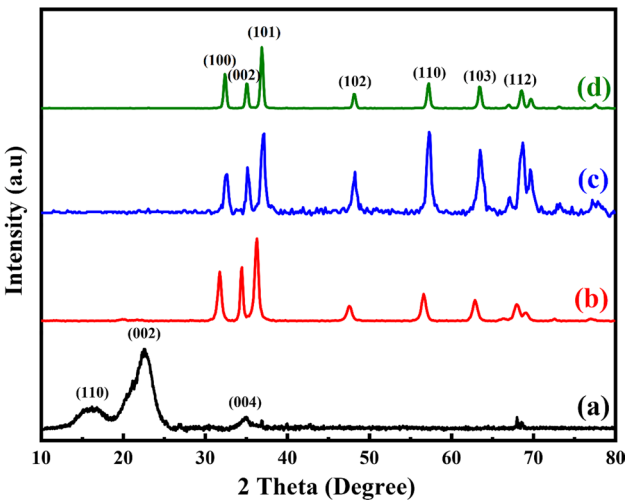

Fig. 3 XRD patterns of (a) Cs, (b) CNC/ZnO NPs.M1, (c) CNC/ZnO NPs.M2, and (d) ZnO NPs

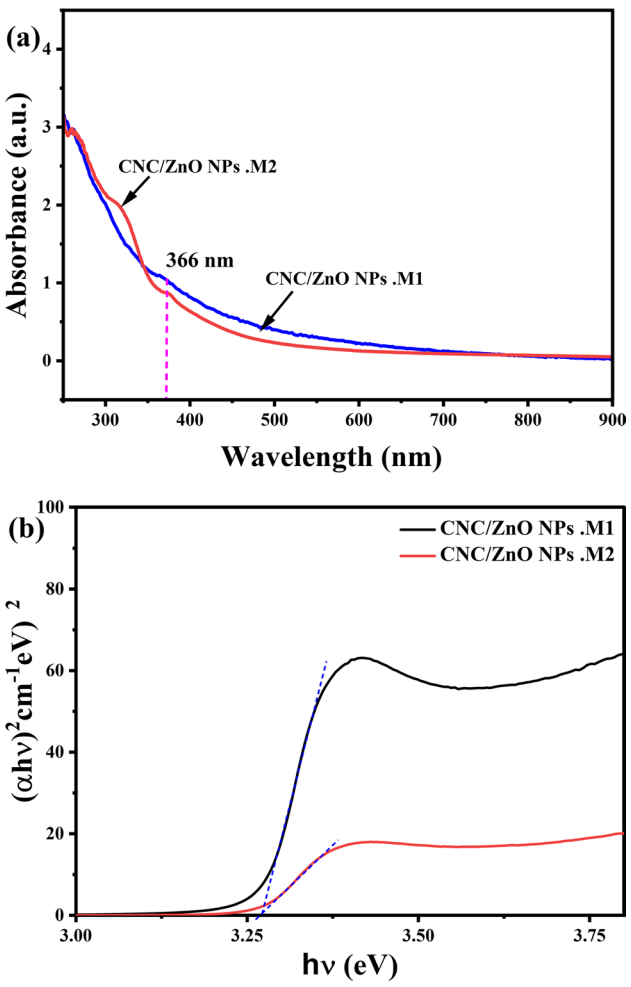

Fig. 4 **a** UV–Vis absorption spectrum, **b** plots of $(\alpha h\upsilon)^2$ versus hυ of CNC/ZnO NPs.M1 and CNC/ZnO NPs.M2.

Tauc relationship between the optical absorption coefficient (α), the photon energy (hv), the constant (A), and the direct bandgap energy (eg). In Fig. 4b, it was found to have a band gap energy value of 3.66 eV for the ZnO NPs synthesized by the two methods, which is in correlation with the previously reported value [73]. For example, differences in different ratios may be due to differences in average crystal size in NPs.

3.4 Morphological investigation

The surface morphology of samples is a very important tool to investigate their microstructure. SEM was used to investigate the shape and morphology of the CNC/ZnO NPs. Figure 5a–d show SEM images of ZnO installed on the surface of CNCs extracted from peanut shells. The ZnO on the surface of the CNCs was different between the two methods. In the sample manufactured in the first method, Fig. 5a–c, the general surface structure shows that the CNCs are smooth and light gray and completely and uniformly covered with spherical-shaped granules without any cracks or pores. The positioning of ZnO on the surface of the CNCs in this way indicates that it is dominant on the surface of CNC/ZnO NPs. Further analysis of CNC/ZnO NPs.M1 by EDAX, as shown in Fig. 6a confirms the associated data, the presence of zinc and oxygen, with a weight ratio of approximately 56.93% Zn and 26.22% O indicating the presence of zinc oxide in addition to the weight ratio of the affinity 16.85% C indicating the presence of cellulose.

In the sample manufactured by the second method in Fig. 5b–d, the results showed a separate and heterogeneous random positioning of white spots on a dark gray mesh background. This gray lattice corresponds to CNC particles, and white spots in hexagonal shapes with smooth surfaces dispersed are ZnO NPs. In this method, the growth of ZnO NPs on of CNCs was at a lower percentage. This is confirmed by the additional analysis by EDAX (Fig. 6b), in which zinc was in a weight ratio of approximately 13.69% which is much less than the first sample.

3.5 Evaluation of the antibacterial and antifungal activities of CNC/ZnO NPs

In this study, the antibacterial activity was qualitatively assessed according to the presence of a zonal inhibitor and the zonal diameter (IZ) compared to *levofloxacin*. This aims to look for the susceptibility of the strains to the studied samples and the antibiotics presented in Fig. 7 can be observed from the formation of clear areas. The clear area is the area covered by bacteria and yeast, so it is denoted as the zone of bacterial inhibition (IZ) (Table 2).

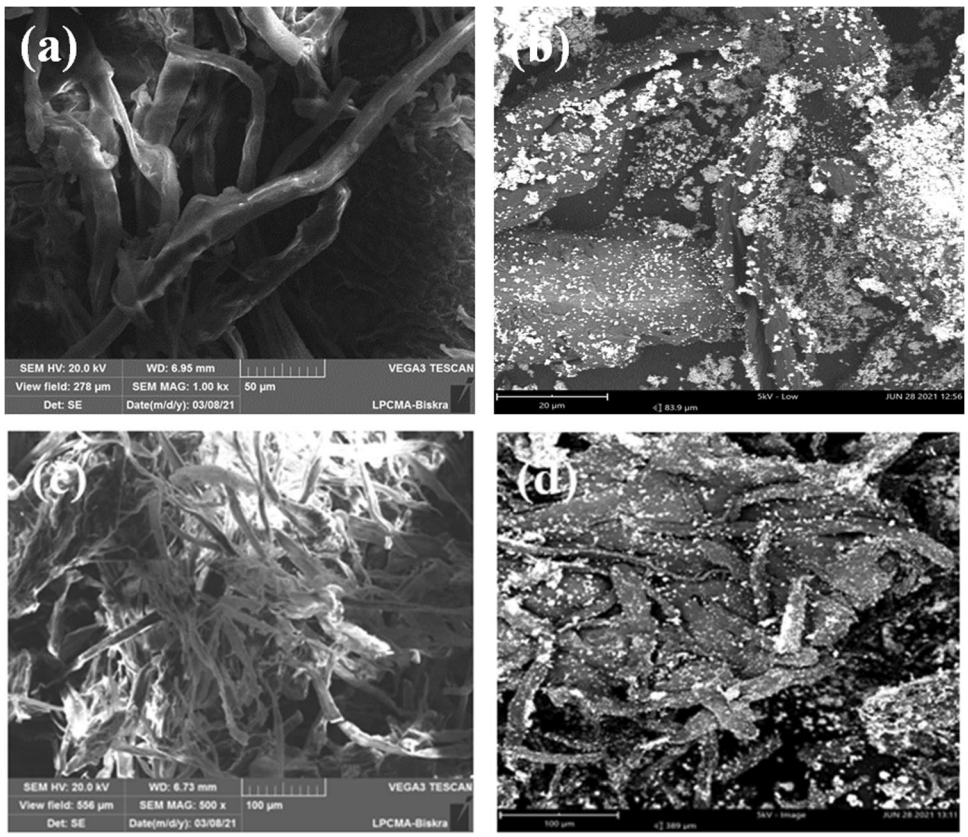

Fig. 5 SEM image: **a**, **c** CNC/ZnO NPs.M1; **b**, **d** of CNC/ZnO NPs.M2

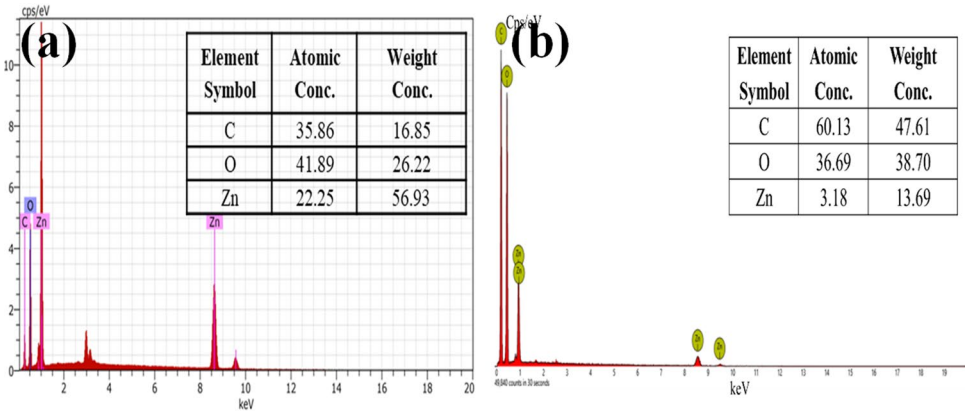

Fig. 6 EDAX: **a**CNC/ZnO NPs. M1; **b** CNC/ZnO NPs.M2

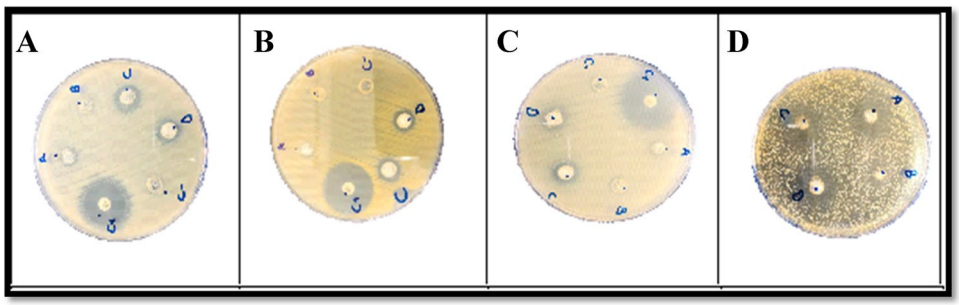

Fig. 7 Antibacterial and antifungal activity of samples by well diffusion method. **A** *Escherichia coli*; **B** *Klebsiella pneumonia*; **C** *Staphylococcus aures*; **D** *Candida albicans*

Table 2 The inhibition zone of antibacterial and antifungal activity of the samples by well diffusion method (inhabitation zones are given in mm)

Activity:	Antibacterial			Antifungal
Bacterial strains:	*Escherichia coli ATCC 25,922*	*Klebsiella pneumonia* ATCC 10,031	*Staphylococcus aureus* ATCC 25,923	*Candida albicans* ATCC 14,053
ZnO NPs	7.16 ± 0.235	7.16 ± 0.235	6.83 ± 0.235	14.33 ± 0.471
CNCs	7 ± 0.00	6.83 ± 0.235	7.16 ± 0.235	8.16 ± 0.235
CNC/ZnO NPs M1	10.33 ± 0.471	11.33 ± 0.471	11 ± 0.00	16.66 ± 0.471
CNC/ZnO NPs M2	11.33 ± 0.471	11 ± 0.00	9.33 ± 0.471	19.66 ± 0.471
Levofloxacin	29.33 ± 0.471	22.66 ± 0.471	27.66 ± 0.471	/
DMSO	/	/	/	/

The ZNI indicated the effectiveness of biocomposites inhibiting bacteria. The wider the clear zone, the better the ability of biocomposite to inhibit bacterial [74].

The obtained results showed that CNCs hybridized with ZnO NPs prepared by both methods have a positive reaction and close sensitivity against all three tested Gram (−) and Gram (+) strains, as the results of both samples are close and have almost the same intensity of effect (ranging from 9 to 11 mm). About the antifungal activity, it showed a strong sensitivity against *Candida albicans*, as the sample prepared by the second method showed a higher inhibition (19 mm) than the sample prepared by the first method (17 mm). This confirms that CNC/ZnO NPs extracted from peanut shells have antibacterial and antifungal properties, whereas the antibiotic used in general represented a strong inhibition of all tested bacterial strains except for *Candida albicans*. Although this inhibition varies from one strain to another, it remains superior to studied samples.

Antimicrobials are defined as substances used to destroy microorganisms or prevent their growth and include antibiotics and other antibacterial and antifungal agents.

From these results, the addition of ZnO NPs was proven to be able to increase the ability of CNCs to inhibit bacteria by 3 to 4 mm in the IZ, and to inhibit fungi by 8.5 mm and 11.5 mm in the IZ in CNC/ZnO NPs.M1 and CNC/ZnO NPs. M2, respectively. On the other hand, the addition of ZnO NPs more percentage to CNCs did not show an increment in the area of inhibition. This could be due to the limited ability

of ZnO NPs to bind CNCs. Based on the chemical structure of CNCs and ZnO NPs, the bonds that occurred in the biocomposite are strong hydrogen bonds between the hydroxyl group of ZnO NPs dissolved in water and the hydroxyl group of CNCs. From the dissolution difficulty of CNCs and ZnO NPs, it cannot bind all CNCs by ZnO NPs[75].

The biocomposite mixture is thought to be able to inhibit microbes by destroying the structure of cell walls and denaturing proteins, resulting in enzyme deactivation [76–78].

This happens because the process of inhibiting the growth of microorganisms is generally caused by several things including the presence of disruptive compounds on the cell walls, causing increased cell membrane permeability resulting in loss of cell components, inactivity of enzymes in cells, and the process of destruction or damage to genetic material [79, 80].

According to Candan et al. [81], the effect of water-soluble substances is weaker than that of water-insoluble substances. This may indicate that water-insoluble compound molecules can insert themselves into and disrupt bacterial cell membranes.

Padmavathy et al. [82], ZnO NPs also have an abrasive surface roughness that impairs the antibacterial process and destroys the bacterial membrane of both Grampositive and Gram-negative bacteria.

Jones et al. investigated the antibacterial activity of ZnO, TiO_2, CuO, CeO_2, $Al2O_3$, and MgO against the bacterium *Staphylococcus aureus* and compared their antibacterial activities. The ZnO NPs were among them and showed significant growth inhibition [83].

Yamamoto et al. investigated the ability of *Escherichia coli* and *Staphylococcus aureus* to control bacteria cultured in an infusion medium to the influence of ZnO NPs size. It was found that the antibacterial activity increased with decreasing particle size. Regarding our antifungal activity results, they are interesting. Therefore, it is necessary and beneficial to develop natural products with antibacterial activity [84].

The biocomposite CNC/ZnO NPs.M2 was chosen to be the most optimum sample with the optical and morphological properties with anti-microbial activities tested.

4 Conclusion

Cellulose is the most abundant biopolymer on earth, being the main structural component of the plant cell wall, with chemical functional groups that can be modified for the purpose of using it in a variety of useful applications.

The originality of this work is based on the recycling of plant waste represented in peanut shells. In this work, CNCs were extracted from peanut shells by acid treatment method using different concentrations of H_2SO_4 solution (36%, 38%, and 40%) as a shape, size, and crystallinity index.

The particle size of CNCs from different C_{H2SO4} = (36%, 38%, and 40%) are 11.82 nm, 11.90 nm, and 8.88 nm, and the crystallinity index is 69.71%, 68.75%, and 77.95%, respectively.

Then, the CNC/ZnO NP compound was prepared by two different methods. In the first stage, we relied on the first method of dissolving cellulose in a basic solution, while in the second method we used cellulose crystals directly without dissolving them. In the second stage, ZnO NPs were prepared by sol–gel synthesis method on the CNCs. The particle size of CNC/ZnO NPs from the first method and second methods is 20.14 nm and 27.31 nm, and the band gap energies are 3.66 eV and 3.66 eV, respectively.

The obtained CNC/ZnO NPs showed good antimicrobial activity and were significantly more resistant in yeast than in Gram-positive and Gram-negative bacteria. A decrease in the antimicrobial activity was observed in the sample prepared by the first method, which contained a higher proportion of zinc particles (in EDAX) although it had a lower particle size, which indicates a possible mechanism of antibacterial action, where direct contact with cell walls leads to the release of Zn^{+2} ions from the CNC/ZnO NPs in limited locations to inhibit microbes by destroying the structure of the cell wall.

In conclusion, from the current study, these results indicate that the CNC/ZnO NPs tested in this study by both methods contain potential antimicrobial components that may be of great benefit in the development of antimicrobial pharmaceutical industries and can be used as a treatment against various diseases caused by these bacteria. It can also be used as a natural preservative for food to eliminate or control the growth of spoilage and disease-causing microorganisms.

The present findings will form a basis for selecting certain plant species for further investigation of the potential discovery of new bioactive natural compounds for it to be beneficial to conduct further studies to better evaluate the potential efficacy of this compound as an anti-microbial agent.

Also, based on these results, there is also a need to develop more innovative techniques to modify nano-cellulosic composites based on metal oxides as materials of interest for a wide range of applications. They can be used as multifunctional nanomaterials as solar photocatalysts, cells, wastewater treatment, photodetector, and sensors with potential applications in coatings, biomedical, and packaging materials.

Author contribution Conceptualization: H.T., D.S., and A.B., and O.B.M; methodology: H.T., A.B., and O.B.M; software: H.T., D.S., and A.B.; validation: A.B., D.S., and O.B.M; formal analysis: H.T., A.R., and D.S.; investigation: A.B.; resources: H.T., A.R.; data curation:

H.T.; writing—original draft preparation: H.T., D.S., and A.B., and O.B.M; writing—review and editing: H.T., D.S., A.B., and O.B.M; supervision: H.T., A.R.; the authors have read and agreed to the published version of the manuscript.

Funding Not applicable.

Data availability and materials Not applicable.

Declarations

Ethical approval Not applicable.

Conflict of interest The authors declare no competing interests.

References

1. Cruz DM, Mostafavi E, Vernet-Crua A, Barabadi H, Shah V, Cholula-Díaz JL, Guisbiers G, Webster TJ (2020) Green nanotechnology-based zinc oxide (ZnO) nanomaterials for biomedical applications: a review. J Phys: Mater 3(3):034005
2. Gao Y, Xu D, Ren D, Zeng K, Wu X (2020) Green synthesis of zinc oxide nanoparticles using Citrus sinensis peel extract and application to strawberry preservation: a comparison study. Lwt 126:109297
3. Bouafia A, Laouini SE (2020) Green synthesis of iron oxide nanoparticles by aqueous leaves extract of Mentha Pulegium L.: effect of ferric chloride concentration on the type of product. Mater Lett 265:127364. https://doi.org/10.1016/j.matlet.2020.127364
4. Bouafia A, Laouini SE, Ahmed ASA, Soldatov AV, Algarni H, Feng Chong K, Ali GAM (2021) The recent progress on silver nanoparticles: synthesis and electronic applications. Nanomater 11(9):2318
5. Bouafia A, Laouini SE, Khelef A, Tedjani ML, Guemari F (2021) Effect of Ferric Chloride Concentration on the Type of Magnetite (Fe3O4) Nanoparticles biosynthesized by aqueous leaves extract of artemisia and assessment of their antioxidant activities. J Cluster Sci 32(4):1033–1041. https://doi.org/10.1007/s10876-020-01868-7
6. Galoppini E, Rochford J, Chen H, Saraf G, Lu Y, Hagfeldt A, Boschloo G (2006) Fast electron transport in metal organic vapor deposition grown dye-sensitized ZnO nanorod solar cells. J Phys Chem B 110(33):16159–16161
7. Zhang Q, Zhang S, Xie C, Zeng D, Fan C, Li D, Bai Z (2006) Characterization of Chinese vinegars by electronic nose. Sens Actuators, B Chem 119(2):538–546
8. Height MJ, Pratsinis SE, Mekasuwandumrong O, Praserthdam P (2006) Ag-ZnO catalysts for UV-photodegradation of methylene blue. Appl Catal B 63(3–4):305–312
9. Liu R, Ye H, Xiong X, Liu H (2010) Fabrication of TiO2/ZnO composite nanofibers by electrospinning and their photocatalytic property. Mater Chem Phys 121(3):432–439
10. Yin Z, Sun S, Salim T, Wu S, Huang X, He Q, Lam YM, Zhang H (2010) Organic photovoltaic devices using highly flexible reduced graphene oxide films as transparent electrodes. ACS Nano 4(9):5263–5268
11. Amornpitoksuk P, Suwanboon S, Sangkanu S, Sukhoom A, Wudtipan J, Srijan K, Kaewtaro S (2011) Synthesis, photocatalytic and antibacterial activities of ZnO particles modified by diblock copolymer. Powder Technol 212(3):432–438
12. Zhang L, Ding Y, Povey M, York D (2008) ZnO nanofluids–a potential antibacterial agent. Prog Nat Sci 18(8):939–944
13. Tam K, Djurišić A, Chan C, Xi Y, Tse C, Leung Y, Chan W, Leung F, Au D (2008) Antibacterial activity of ZnO nanorods prepared by a hydrothermal method. Thin Solid Films 516(18):6167–6174
14. Stoimenov PK, Klinger RL, Marchin GL, Klabunde KJ (2002) Metal oxide nanoparticles as bactericidal agents. Langmuir 18(17):6679–6686
15. Seddiqi H, Oliaei E, Honarkar H, Jin J, Geonzon LC, Bacabac RG, Klein-Nulend J (2021) Cellulose and its derivatives: towards biomedical applications. Cellulose 28(4):1893–1931
16. Collazo-Bigliardi S, Ortega-Toro R, Boix AC (2018) Isolation and characterisation of microcrystalline cellulose and cellulose nanocrystals from coffee husk and comparative study with rice husk. Carbohyd Polym 191:205–215
17. Trache D, Hussin MH, Chuin CTH, Sabar S, Fazita MN, Taiwo OF, Hassan T, Haafiz MM (2016) Microcrystalline cellulose: isolation, characterization and bio-composites application—a review. Int J Biol Macromol 93:789–804
18. Azizi S, Ahmad M, Mahdavi M, Abdolmohammadi S (2013) Preparation, characterization, and antimicrobial activities of ZnO nanoparticles/cellulose nanocrystal nanocomposites. BioRes 8(2):1841–1851
19. Li J, Wei X, Wang Q, Chen J, Chang G, Kong L, Su J, Liu Y (2012) Homogeneous isolation of nanocellulose from sugarcane bagasse by high pressure homogenization. Carbohyd Polym 90(4):1609–1613
20. Ribeiro RS, Pohlmann BC, Calado V, Bojorge N, Pereira N Jr (2019) Production of nanocellulose by enzymatic hydrolysis: trends and challenges. Eng Life Sci 19(4):279–291
21 Wulandari W, Rochliadi A, Arcana I (2016) Nanocellulose prepared by acid hydrolysis of isolated cellulose from sugarcane bagasse. IOP Conf Ser Mater Sci Eng 107:012045
22. Shahi N, Min B, Sapkota B, Rangari VK (2020) Eco-friendly cellulose nanofiber extraction from sugarcane bagasse and film fabrication. Sustain 12(15):6015
23. De Souza Lima MM, Wong JT, Paillet M, Borsali R, Pecora R (2003) Translational and rotational dynamics of rodlike cellulose whiskers. Langmuir 19(1):24–29
24. Nishino T, Matsuda I, Hirao K (2004) All-cellulose composite Macromelcules 37:7683–7687
25. Šturcová A, Davies GR, Eichhorn SJ (2005) Elastic modulus and stress-transfer properties of tunicate cellulose whiskers. Biomacromol 6(2):1055–1061
26. He J, Kunitake T, Nakao A (2003) Facile in situ synthesis of noble metal nanoparticles in porous cellulose fibers. Chem Mater 15(23):4401–4406
27. Liu H, Wang D, Song Z, Shang S (2011) Preparation of silver nanoparticles on cellulose nanocrystals and the application in electrochemical detection of DNA hybridization. Cellulose 18(1):67–74
28. Huber P (1998) Recueil de fiches techniques d'Agriculture Spéciale 17:23–27
29. Anggrianto K, Salea R, Veriansyah B, Tjandrawinata RR (2014) Application of supercritical fluid extraction on food processing: black-eyed pea (Vigna unguiculata) and peanut (Arachis hypogaea). Procedia Chemistry 9:265–272
30. Pattee HE (2005) Peanut oil. Bailey's Industrial Oil and Fat Products 2:431À464
31. Szymańska-Chargot M, Chylińska M, Gdula K, Kozioł A, Zdunek A (2017) Isolation and characterization of cellulose from different fruit and vegetable pomaces. Polymers 9(10):495
32. Kouadri I, Satha H (2018) Extraction and characterization of cellulose and cellulose nanofibers from Citrullus colocynthis seeds. Ind Crops Prod 124:787–796
33. Abdullah JAA, Eddine LS, Abderrhmane B, Alonso-González M, Guerrero A, Romero A (2020) Green synthesis and characterization of iron oxide nanoparticles by pheonix dactylifera leaf extract and evaluation of their antioxidant activity. Sustain Chem Pharm 17:100280

34. Abderrhmane B, Salah Eddine L (2020) Plant-mediated synthesis of iron oxide nanoparticles and evaluation of the antimicrobial activity: a review. Mini-Rev Org Chem 17:1–10. https://doi.org/10.2174/1570193X17999200908091139
35. Bouafia A, Laouini SE, Ouahrani MR (2020) A review on green synthesis of CuO nanoparticles using plant extract and evaluation of antimicrobial activity. Asian J Res Chem 13(1):65–70
36. Laouini SE, Bouafia A, Soldatov AV, Algarni H, Tedjani ML, Ali GAM, Barhoum A (2021) Green synthesized of Ag/Ag2O nanoparticles using aqueous leaves extracts of Phoenix dactylifera L. and Their Azo Dye Photodegradation. Membr 11(7):468
37. Bouafia A, Laouini SE, Tedjani ML, Ali GAM, Barhoum A (2021) Green biosynthesis and physicochemical characterization of Fe3O4 nanoparticles using Punica granatum L. fruit peel extract for optoelectronic applications. Text Res J 97(15):2685–2696. https://doi.org/10.1177/00405175211006671
38. Daoudi H, Bouafia A, Meneceur S, Laouini SE, Belkhalfa H, Lebbihi R, Selmi B (2022) Secondary metabolite from Nigella sativa seeds mediated synthesis of silver oxide nanoparticles for efficient antioxidant and antibacterial activity. J Inorg Organomet Polym Mater 32(11):4223–4236. https://doi.org/10.1007/s10904-022-02393-y
39. Meneceur S, Hemmami H, Bouafia A, Laouini SE, Tedjani ML, Berra D, Mahboub MS (2022) Photocatalytic activity of iron oxide nanoparticles synthesized by different plant extracts for the degradation of diazo dyes Evans blue and Congo red. Biomass Convers Biorefinery.https://doi.org/10.1007/s13399-022-02734-4
40. Cai J, Zhang L (2005) Rapid dissolution of cellulose in LiOH/urea and NaOH/urea aqueous solutions. Macromol Biosci 5(6):539–548
41. Megashah LN, Ariffin H, Zakaria MR, Hassan MA, Andou Y, Padzil FNM (2020) Modification of cellulose degree of polymerization by superheated steam treatment for versatile properties of cellulose nanofibril film. Cellulose 27(13):7417–7429
42. Patterson A (1939) The Scherrer formula for X-ray particle size determination. Phys Rev 56(10):978
43. Ranganagowda R, Kamath S, Bennehalli B (2019) Extraction and characterization of cellulose from natural Areca fiber. Mat Sci Res India 16:86–93
44. Berra D, Laouini S, Benhaoua B, Ouahrani M, Berrani D, Rahal A (2018) Green synthesis of copper oxide nanoparticles by Pheonix dactylifera L leaves extract. Dig J Nanomater Biostruct 13(4):1231–1238
45. Bazerque P, Perez C, Pauli M (1990) Antibiotic assay by the agar-well diffusion method. Acta Biol Med Exp 15:113–115
46. Prasad RN, Viswanathan S, Devi JR, Nayak V, Swetha V, Archana B, Parathasarathy N, Rajkumar J (2008) Preliminary phytochemical screening and antimicrobial activity of Samanea saman. J Med Plants Res 2(10):268–270
47. Manimaran P, Pillai GP, Vignesh V, Prithiviraj M (2020) Characterization of natural cellulosic fibers from Nendran Banana Peduncle plants. Int J Biol Macromol 162:1807–1815
48. Ravindran D, SR SB, Indran S (2020) Characterization of surface-modified natural cellulosic fiber extracted from the root of Ficus religiosa tree. Int J Biol Macromol 156:997–1006
49. Yunil H, Lilik N, Rohmawati H (2021) Antibacterial activity of sugarcane Bagasse nanocellulose biocomposite with chitosan against *Escherichia coli*. Jurnal Kimia Valensi (Jurnal Kimia VALENSI, volume 7, no 1, May 2021):28–37
50. Boumediri H, Bezazi A, Del Pino GG, Haddad A, Scarpa F, Dufresne A (2019) Extraction and characterization of vascular bundle and fiber strand from date palm rachis as potential bio-reinforcement in composite. Carbohyd Polym 222:114997
51. Khiari R, Rol F, Salon MB, Bras J, Belgacem M (2019) ACS sustainable chem Eng 7:8155–8167
52. Loganathan TM, Sultan MTH, Ahsan Q, Jawaid M, Naveen J, Shah AUM, Hua LS (2020) Characterization of alkali treated new cellulosic fibre from Cyrtostachys renda. J Market Res 9(3):3537–3546
53. Narayanasamy P, Balasundar P, Senthil S, Sanjay M, Siengchin S, Khan A, Asiri AM (2020) Characterization of a novel natural cellulosic fiber from Calotropis gigantea fruit bunch for eco-friendly polymer composites. Int J Biol Macromol 150:793–801
54. Mansour R, Abdelaziz A, Fatima Zohra A (2018) Characterization of long lignocellulosic fibers extracted from L. leaves. Research Journal of Textile and Apparel 22 (3):195–211. https://doi.org/10.1108/RJTA-02-2018-0009
55. Vinod A, Vijay R, Singaravelu DL, Sanjay M, Siengchin S, Moure M (2019) Characterization of untreated and alkali treated natural fibers extracted from the stem of Catharanthus roseus. Mater Res Expr 6(8):085406
56. Kim SH, Lee CM, Kafle K (2013) Characterization of crystalline cellulose in biomass: basic principles, applications, and limitations of XRD, NMR, IR, Raman, and SFG. Korean J Chem Eng 30(12):2127–2141
57. Zaman M, Xiao H, Chibante F, Ni Y (2012) Synthesis and characterization of cationically modified nanocrystalline cellulose. Carbohyd Polym 89(1):163–170
58. Zannen S, Ghali L, Halimi M, Hssen MB (2014) Effect of chemical extraction on physicochemical and mechanical properties of doum palm fibres. Adv Mater Phys Chem 4(10):203
59. Mo Z-l, Zhao Z-l, Chen H, Niu G-p, Shi H-f (2009) Heterogeneous preparation of cellulose–polyaniline conductive composites with cellulose activated by acids and its electrical properties. Carbohyd Polym 75(4):660–664
60. Zak AK, Abrishami ME, Majid WA, Yousefi R, Hosseini S (2011) Effects of annealing temperature on some structural and optical properties of ZnO nanoparticles prepared by a modified sol–gel combustion method. Ceram Int 37(1):393–398
61. Vijay R, Singaravelu DL, Vinod A, Sanjay M, Siengchin S, Jawaid M, Khan A, Parameswaranpillai J (2019) Characterization of raw and alkali treated new natural cellulosic fibers from Tridax procumbens. Int J Biol Macromol 125:99–108
62. Saravanakumar S, Kumaravel A, Nagarajan T, Sudhakar P, Baskaran R (2013) Characterization of a novel natural cellulosic fiber from Prosopis juliflora bark. Carbohyd Polym 92(2):1928–1933
63. Liu R, Yu H, Huang Y (2005) Structure and morphology of cellulose in wheat straw. Cellulose 12(1):25–34
64. Mayandi K, Rajini N, Pitchipoo P, Sreenivasan V, Jappes JW, Alavudeen A (2015) A comparative study on characterisations of Cissus quadrangularis and Phoenix reclinata natural fibres. J Reinf Plast Compos 34(4):269–280
65. Ilyas RA, Sapuan SM, Kadier A, Krishnan S, Atikah MSN, Ibrahim R, Nazrin A, Syafiq R, Misri S, Huzaifah MRM, Hazrol MD (2020) Chapter 7 - Mechanical testing of sugar palm fiber reinforced sugar palm biopolymer composites. In: Al-Oqla FM, Sapuan SM (eds) Advanced processing, properties, and applications of starch and other bio-based polymers. Elsevier, pp 89–110. https://doi.org/10.1016/B978-0-12-819661-8.00007-X
66. Cheng D, Weng B, Chen Y, Zhai S, Wang C, Xu R, Guo J, Lv Y, Shi L, Guo Y (2020) Characterization of potential cellulose fiber from Luffa vine: a study on physicochemical and structural properties. Int J Biol Macromol 164:2247–2257
67. Adel Salih A, Zulkifli R, Azhari CH (2020) Tensile properties and microstructure of single-cellulosic bamboo fiber strips after alkali treatment. Fibers 8(5):26
68. Jiang Y, Deng P, Jing L, Zhang T (2019) Tensile properties and structure characterization of palm fibers by alkali treatment. Fibers Polym 20(5):1029–1035
69. Getie S, Belay A, Ar CR, Belay Z (2017) Synthesis and characterizations of zinc oxide nanoparticles for antibacterial applications. J Nanotechnology 8:1–8

70. Suryanto H, Marsyahyo E, Irawan YS, Soenoko R (2014) Effect of alkali treatment on crystalline structure of cellulose fiber from mendong (Fimbristylis globulosa) straw. Key Engineering Materials. Trans Tech Publ, pp 720–724
71. Wang H, Xie C (2008) Effect of annealing temperature on the microstructures and photocatalytic property of colloidal ZnO nanoparticles. J Phys Chem Solids 69(10):2440–2444
72. Mahamuni PP, Patil PM, Dhanavade MJ, Badiger MV, Shadija PG, Lokhande AC, Bohara RA (2019) Synthesis and characterization of zinc oxide nanoparticles by using polyol chemistry for their antimicrobial and antibiofilm activity. Biochem Biophys Rep 17:71–80
73. Xaba T, Mongwai PP, Lesaoana M (2019) Decomposition of Bis(N-benzyl-salicydenaminato)zinc (II) complex for the synthesis of ZnO nanoparticles to fabricate ZnO-chitosan nanocomposite for the removal of Iron (II) ions from wastewater. Journal of Chemistry 2019:1907083. https://doi.org/10.1155/2019/1907083
74. Szymańska-Chargot M, Chylińska M, Pertile G, Pieczywek PM, Cieślak KJ, Zdunek A, Frąc M (2019) Influence of chitosan addition on the mechanical and antibacterial properties of carrot cellulose nanofibre film. Cellul 26(18):9613–9629
75. Ak HPS, Saurabh CK, Adnan A, Fazita MN, Syakir M, Davoudpour Y, Rafatullah M, Abdullah C, Haafiz M, Dungani R (2016) A review on chitosan-cellulose blends and nanocellulose reinforced chitosan biocomposites: properties and their applications. Carbohyd Polym 150:216–226
76. Calcott PH (1982) Cyclic AMP and cyclic GMP control of synthesis of constitutive enzymes in Escherichia coli. Microbiol 128(4):705–712
77. Nieß A, Siemann-Herzberg M, Takors R (2019) Protein production in Escherichia coli is guided by the trade-off between intracellular substrate availability and energy cost. Microb Cell Fact 18(1):1–10
78. Kim SH, Schneider BL, Reitzer L (2010) Genetics and regulation of the major enzymes of alanine synthesis in Escherichia coli. J Bacteriol 192(20):5304–5311
79. Kontiza I, Stavri M, Zloh M, Vagias C, Gibbons S, Roussis V (2008) New metabolites with antibacterial activity from the marine angiosperm Cymodocea nodosa. Tetrahedron 64(8):1696–1702
80. Paramita DAK, Antara NS, Gunam IBW (2014) Inhibition activity of essential oil of lemongrass leaves (Cymbopogon citratus) on the growth of Escherichia coli, Staphylococcus aureus, AND Vibrio cholerae. Jurnal Rekayasa Dan Manajemen Agroindustri 2(1):29–38
81. Candan F, Unlu M, Tepe B, Daferera D, Polissiou M, Sökmen A, Akpulat HA (2003) Antioxidant and antimicrobial activity of the essential oil and methanol extracts of Achillea millefolium subsp. millefolium Afan.(Asteraceae). J Ethnopharmacol 87(2–3):215–220
82. Padmavathy N, Vijayaraghavan R (2008) Enhanced bioactivity of ZnO nanoparticles—an antimicrobial study. Sci Technol Adv Mater 9(3):035004. https://doi.org/10.1088/1468-6996/9/3/035004
83. Abebe B, Murthy HA, Zerefa E, Adimasu Y (2020) PVA assisted ZnO based mesoporous ternary metal oxides nanomaterials: synthesis, optimization, and evaluation of antibacterial activity. Mater Res Expr 7(4):045011
84. Bougherra HH, Bedini S, Flamini G, Cosci F, Belhamel K, Conti B (2015) Pistacia lentiscus essential oil has repellent effect against three major insect pests of pasta. Ind Crops Prod 63:249–255